

STELLAR PARAMETERS AND RADIAL VELOCITIES OF HOT STARS IN THE CARINA
NEBULA

RICHARD J. HANES,¹ M. VIRGINIA MCSWAIN,¹ AND MATTHEW S. POVICH²

¹*Department of Physics, Lehigh University, 16 Memorial Drive East, Bethlehem, PA 18015, USA*

²*Department of Physics & Astronomy, California State Polytechnic University Polytechnic, Pomona, CA 91768, USA*

ABSTRACT

The Carina Nebula is an active star forming region in the southern sky that is of particular interest due to the presence of a large number of massive stars in a wide array of evolutionary stages. Here we present the results of the spectroscopic analysis of 82 B-type stars and 33 O-type stars that were observed in 2013 and 2014. For 82 B-type stars without line blending, we fit model spectra from the Tlusty BSTAR2006 grid to the observed profiles of H γ and He $\lambda\lambda$ 4026, 4388, and 4471 to measure the effective temperatures, surface gravities, and projected rotational velocities. We also measure the masses, ages, radii, bolometric luminosities, and distances of these stars. From the radial velocities measured in our sample, we find 31 single lined spectroscopic binary candidates. We find a high dispersion of radial velocities among our sample stars, and we argue that the Carina Nebula stellar population has not yet relaxed and become virialized.

Keywords: stars: fundamental parameters – stars: massive – binaries: spectroscopic –
open clusters and associations: individual (Carina)

rjh314@lehigh.edu

mcswain@lehigh.edu

1. INTRODUCTION

The Carina Nebula is one of the most active star forming regions located nearby in our Galaxy, containing many massive stars spanning across the evolutionary spectrum. The brightness, proximity, and size of Carina (more than 1 deg^2 on the sky) make it an ideal candidate for study as it provides a window into the entire stellar formation and evolution process. It has been the subject of several recent, large surveys including the Chandra Carina Complex Project (CCCP) (Townsend et al. 2011), the VISTA Carina Nebula Survey (Preibisch et al. 2014), and the VST Photometric H α Survey (VPHAS+) (Mohr-Smith et al. 2017).

With over 200 massive OB stars (Gagné et al. 2011) and 1400 young stellar objects (YSOs; Povich et al. 2011), study of physical parameters of these stars can provide insight into stellar formation across the nebula. Huang & Gies (2006) measured the effective temperature (T_{eff}), surface gravity ($\log g$), projected rotational velocity ($V \sin i$), and helium abundance of 39 stars spread across clusters Collinder (Coll) 228, Trumpler (Tr) 14, and Tr 16 in Carina. Berlanas et al. (2017) recently performed a preliminary study of 14 O-type stars observed in the Gaia-ESO Survey (GES). While both of these studies give an initial look into the spectroscopic parameters of the stars in Carina, there is still a need for a broader study of the stars throughout the rest of the nebula.

In a previous paper (Alexander et al. 2016), we spectroscopically classified 36 O-type stars and 128 B-type stars scattered throughout the nebula, confirming 23 new OB-type stars. We present here the results of the measurements of physical parameters of the observed B stars from Alexander et al. (2016). This paper should provide the current largest and most comprehensive catalog of spectroscopic parameters of massive stars in the Carina Nebula.

Section 2 briefly describes the observations and data reduction of the spectra. In Section 3, we discuss how we measured, via model fitting with the *TLUSTY* BSTAR2006 grid, T_{eff} , $\log g$, and $V \sin i$ of these stars. Comparing these results to the evolutionary tracks and isochrones, we also measure

the mass, radius, and age. We also compare our results with any shared stars in past studies. Section 4 discusses the radial velocities and distances of the stars in our sample.

2. OBSERVATIONS

Observations of the stars were made at the Anglo-Australian Telescope (AAT) over the course of two runs in March 2013 and April 2014. The observations of these stars are described in greater detail by [Alexander et al. \(2016\)](#). We chose two different wavelength regions, 3925-4210 Å (2013) and 4235-4510 Å (2014), to cover many useful H and He lines for analysis. As the target spectra were vertically stacked on the imaging plane, distortions in the imaging plane meant that the exact spectral coverage varied among the targets and sky spectra. During our first day of observations in 2014, we used a slightly different range (4200-4475 Å) for some of our exposures, but we found that this omitted the He I λ 4471 line for some of our targets due to variable dispersion across the chip.

The raw spectra were reduced using the DOHYDRA package of IRAF and a custom IDL code for sky subtraction to account for the changing wavelength coverage across the CCD. Due to the variable dusty nature of the Carina Nebula, sometimes the average sky spectrum is too strong or too weak in comparison to our targets, which results in contamination of the Balmer line cores for some of our stars.

Bright stars in our 2013 data generally have a signal-to-noise ratio (S/N) of 50-120, while the faint stars have a S/N of 30-70. The bright stars in our 2014 data have a S/N of 100-200, while the faint stars have a S/N of 120-210. The signal-to-noise of our 2013 data was low because our observing time was cut short due to wildfires in the area. We used two different fiber configurations for the bright versus the faint stars and observed them with different exposure times, which is how we achieved marginally better S/N for the fainter stars. Our measurements of S/N for each star are listed in Table 1.

3. STELLAR PHYSICAL PARAMETERS

We used the non-local thermodynamic equilibrium (NLTE) *TLUSTY* BSTAR2006 (Lanz & Hubeny 2007) model spectra to measure T_{eff} , $\log g$, and $V \sin i$ of our observed B-type stars. BSTAR2006 offers several grids with different metallicities and microturbulent velocities. For our purposes, we assumed a solar metallicity ($Z/Z_{\odot} = 1$) and a microturbulent velocity of $V_t = 2 \text{ km s}^{-1}$. The value for microturbulent velocity is not very important in this situation because He I $\lambda\lambda$ 4471, 4388, and 4026, which we used to measure $V \sin i$, are not very sensitive to V_t (Lyubimkov et al. 2004).

Before fitting the stars, we first estimated the T_{eff} and $\log g$ for a star based on the strength and shape of the Balmer and helium lines in our spectra. Using custom IDL codes, we measure $V \sin i$ by artificially broadening the model spectra for instrumental and rotational broadening across a series of 10 km s^{-1} steps. We then compare the sum of the squares of the residuals ($\Sigma(\text{O-C})^2$) for each step and determine minimal value of a parabolic fit as the value for $V \sin i$ for a given line. The error associated with this measurement was calculated by finding fits that fell at or below a 5% tolerance in $\Sigma(\text{O-C})^2$. We used the He I $\lambda\lambda$ 4026, 4388, and 4471 lines for the fitting process, and then a weighted average is calculated as our measured $V \sin i$. The measurements for $V \sin i$ of all the helium lines as well as the weighted average are recorded in Table 1.

After measuring $V \sin i$, we then modeled the spectra at $\text{H}\gamma$ for T_{eff} and $\log g$ along each point in the BSTAR2006 grid. Once we found the closest fits within grid, we then interpolated between grid points via a linear scaling of the models to find the best fit for T_{eff} and $\log g$. Errors for T_{eff} and $\log g$ were calculated by finding fits that fall at or below a 10% tolerance in the $\Sigma(\text{O-C})^2$ because we fit for the two parameters simultaneously. T_{eff} and $\log g$ are recorded in Table 2.

The earliest B stars have temperatures near $T_{\text{eff}} = 30,000 \text{ K}$, at the edge of the BSTAR2006 grid, resulting in errors in T_{eff} that are likely underestimated. Comparing our measured T_{eff} with the spectral types in Alexander et al. (2016), we note that some of the stars appear hotter than expected. A

hotter B-type star has a smaller $H\gamma$ equivalent width, and their expanding atmospheres will produce emission that will partially fill in the line profile further, making the star appear hotter still. These stars will be analyzed again along with the O-type stars in our sample in a future paper. On the other hand, other B stars appear cooler than expected, which may be a result of unseen binary line blending. Here, the cooler companion's $H\gamma$ profile is artificially increasing the measured line strength. Overall, we find that the temperatures of our earliest B-type stars may be up to 9,000 K cooler than their spectral type suggests, so our formal errors represent only part of the true uncertainty.

Due to the difficulty of sky subtraction and the brightness of Carina in the hydrogen recombination lines, our spectra frequently have nebular contamination at the cores of the Balmer lines that are challenging to properly account for. When present, we ignore the affected wavelengths during the fitting process. This leads to larger errors in our measurements for T_{eff} because we lose information about the line core.

As the effect of $\log g$ is mostly present in the wings of the spectral lines, we find that continuum fitting causes a systematic error of $\Delta \log g_{\text{sys}} \sim 0.1$ dex. To compensate for this systematic error, the errors, $\Delta \log g$, presented in Table 2 are computed using the formal error from our model fitting added in quadrature with the systematic error from the continuum fitting process. We also include an HR-Diagram of our observed stars in Figure 1.

Huang & Gies (2006) performed a similar analysis among a sample of O- and B-type stars in Carina, of which we share 13 B stars. A comparison of our results is shown in Figure 2. Our $V \sin i$ measurements agree within error, with the sole exception of Tr 16-25. We suggest that Tr 16-25 may be a double-lined spectroscopic binary (SB2) considering the large discrepancy between our results. It's possible that the different observation times could have caught the binary system at different stages of the orbit, resulting in different blends of the spectral lines, so measurements of $V \sin i$ would

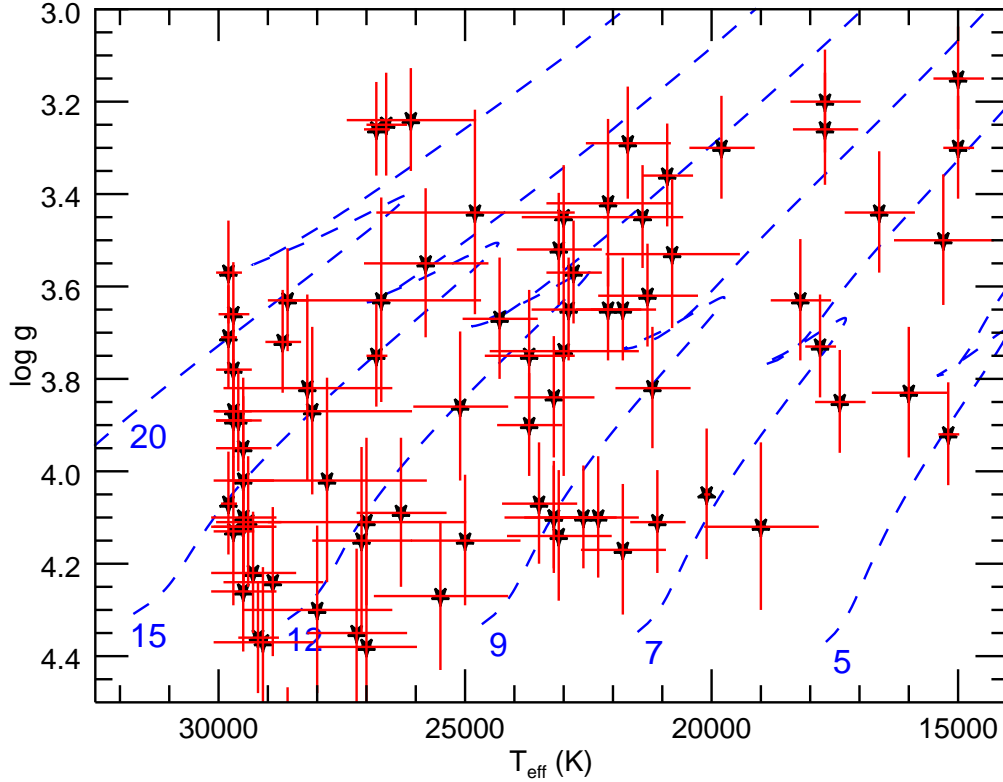
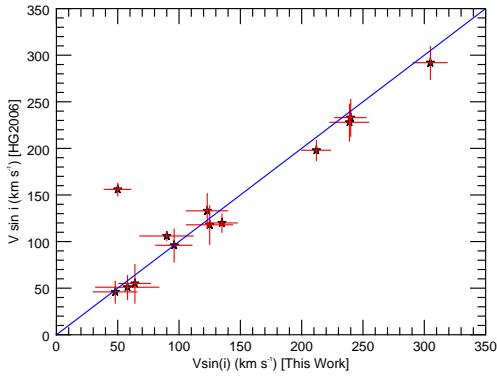


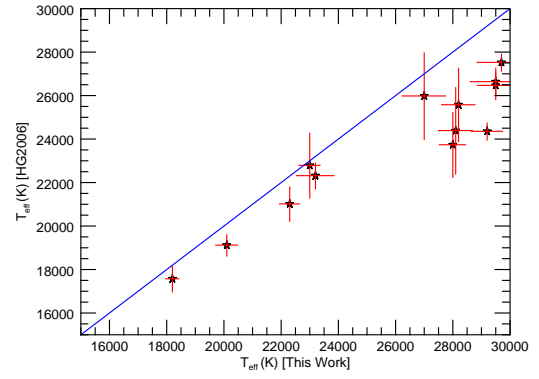
Figure 1. HR-Diagram of our observed B-type stars using the evolutionary tracks offered by [Ekström et al. \(2012\)](#). Stars near $T_{\text{eff}} = 30,000$ K are at the edge of the BSTAR2006 grid and their errors in T_{eff} are likely underestimated. The values associated with each evolutionary track are in solar masses.

differ.

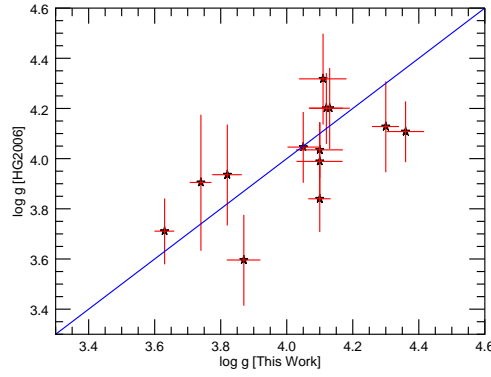
The effective temperatures that we measured seem to have a noticeable increasing trend as the temperature increases. In their paper, [Huang & Gies \(2006\)](#) use the local thermodynamic equilibrium (LTE) ATLAS9 atmospheric models to measure T_{eff} and $\log g$ in contrast to the NLTE Turbulent models we used. It has been shown that LTE models can sufficiently describe cooler stars below $T_{\text{eff}} < 22,000$ K ([Przybilla et al. 2011](#)) and that NLTE models are required for hotter O- and B-type stars. This explains the large discrepancy for our stars with $T_{\text{eff}} > 27,000$ K. Our measurements for



(a)



(b)



(c)

Figure 2. Comparison of our results with Huang & Gies (2006). The horizontal and vertical error bars in these figures are the calculated errors from this work and Huang & Gies (2006), respectively.

$\log g$ are consistent with Huang & Gies (2006).

A straightforward application of our measurements is to compare T_{eff} and $\log g$ to model evolutionary tracks to measure the mass (M_{\star}), radius (R_{\star}), and age (τ_{\star}) of the stars in our sample. Using the non-rotating versions of the evolutionary tracks offered by Ekström et al. (2012), we can measure these parameters by doing a linear interpolation between the evolutionary tracks. These values, as well as the calculated bolometric luminosity (L_{bol}), are included in Table 2. The error bars on each

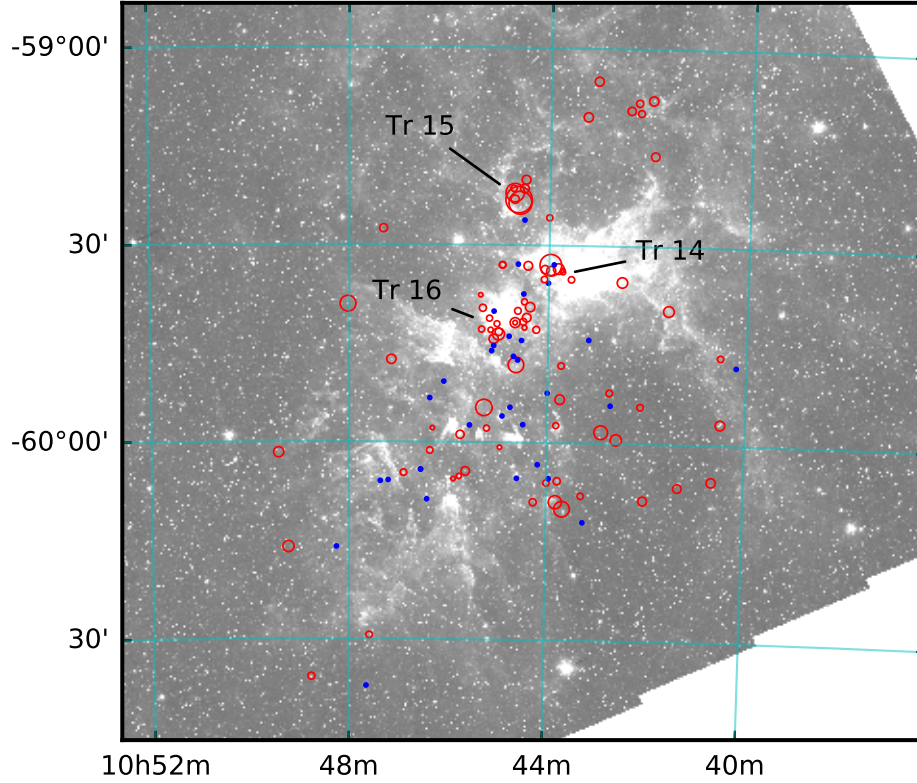


Figure 3. Age distribution of the B stars (red) across Carina. The sizes of the bubbles are relative to the magnitude of the age of the stars. The O stars from our sample are also included in blue. The positions of the clusters Tr 14, Tr 15, and Tr 16 are marked.

quantity are measured by varying T_{eff} and $\log g$ by their respective errors.

As an active star-forming region, the distribution of the stars across the nebula can provide insight into the structure and features of Carina. The stellar age distribution in Figure 3 shows that while there are very young stars scattered throughout the nebula, the oldest B stars in the nebula reside in the Tr 15 cluster. The overall dearth of O-type stars in that cluster, as well as the notably thinner nebulosity in the Tr 15 region, suggest that Tr 15 is the oldest cluster in the nebula. Our results also indicate that Tr 14 is a younger cluster than Tr 16, agreeing with similar conclusions in [Damiani et al. \(2017\)](#) and the WEBDA database.

4. RADIAL VELOCITIES

The public data releases from the Gaia-ESO Survey (GES) have been highly anticipated for their calibrated spectroscopy and derived astrophysical parameters. With this in mind, we measured the radial velocities (V_r) of all observed O and B stars using a simple parabolic or Gaussian fit of the core of the more prominent spectral lines. We used 12 spectral lines¹ across both wavelength regions. Comparing the radial velocities across both epochs, we find that 21 of the 75 (28%) B stars had V_r shifts more than three times the error of the weighted mean V_r . We classify these as single-line spectroscopic binary candidates (SB1c). The results of our radial velocity measurements of the B-type stars can be found in Table 3.

We also include Table 4 which lists the radial velocity measurements of the O-type stars in our sample. These stars are not the intended focus of this publication, but we believe these results will be beneficial for anyone using the GES data releases for analysis of the Carina region. We found 10 of the 31 (32.3%) O stars are SB1 candidates. Further work on the physical parameters of these O-type stars will be forthcoming in a future paper.

To compare the frequency of our detection of SB1 candidates with what we would expect with a year between measurements, we created a simple code to model the radial velocities of O- and B-type stars. We started by choosing random partners and periods for the stars using the IMF indices calculated by [Kiminki & Kobulnicky \(2012\)](#). The inclination angle and phase angle of the orbit were also randomly generated. We assumed a binary fraction of $30\% < \text{B.F.} < 60\%$ following the study by [Kiminki & Kobulnicky \(2012\)](#) for binaries with $P < 1000$ days. We found that we should expect that 19.3 - 38.6% of O- and B-type stars would exhibit large V_r shifts using only two observations with a year between them. This is consistent with our finding that 29.2% (31 of 106) of our observed O- and B- type stars are SB1 candidates.

¹ The lines used for this were He I $\lambda\lambda$ 4009, 4026, 4120, 4144, 4388, and 4471, Si IV $\lambda\lambda$ 4089 and 4116, C II λ 4267, Mg II λ 4481, H δ , and H γ .

In Table 5, we include the radial velocity measurements of the known SB2 systems that we observed that had separate line cores and were not entirely blended together. The radial velocities of the assumed primary star are marked as $V_{r,p}$ while the secondary stars are marked as $V_{r,s}$. The components in HD 303313, HD 93506, LS 1840, and HD 92607 have similar spectral types, making the distinction between the primary and secondary stars impossible.

As a large star forming region, we expect that the stars in Carina will have relatively similar radial velocities, but we find that there is a large V_r dispersion across the nebula. Figure 4 shows the distribution of radial velocities of the observed stars. Known and candidate binaries are not included. Overall, we find that $\langle V_r \rangle = -7.14 \pm 13.10 \text{ km s}^{-1}$ for stars in Carina. The stars HD 93343 and HD 303304 have $|V_r - \langle V_r \rangle| > 30 \text{ km s}^{-1}$ and may be runaway stars from their respective birthplaces. Other stars might also be runaways if their proper motion is sufficiently high.

We show the positional distribution of our radial velocity measurements in Figure 5. About half of the stars with high blueshifts are located far away from their main clusters, suggesting that they may also be runaways. Similarly, the majority of the redshifted stars are located outside of the major clusters, with some being in low extinction (A_V) windows. These stars may also be a runaway population, a background OB population, or a mixture of both.

Carina lies in a complicated part of the Galaxy because it is near the tangent point of the Sagittarius-Carina spiral arm. The recombination and forbidden lines associated with the H II region occupy a larger range of radial velocities (-50 to 50 km s^{-1}) than does our OB population (Damiani et al. 2016). This isn't surprising, given that feedback from the OB stars drives expansion of the nebula. There is a persistent, two-peaked velocity structure in the nebular lines with $(V_{blue}, V_{red}) = (-30, 10) \text{ km s}^{-1} = V_{cm} \pm 20 \text{ km s}^{-1}$ (Damiani et al. 2016). The peak of the velocity distribution of our observed OB stars fits between these two peaks. The densest molecular clouds associated with the Carina Nebula are found toward the negative end of our OB velocities, near -20 km s^{-1} (Rebolledo

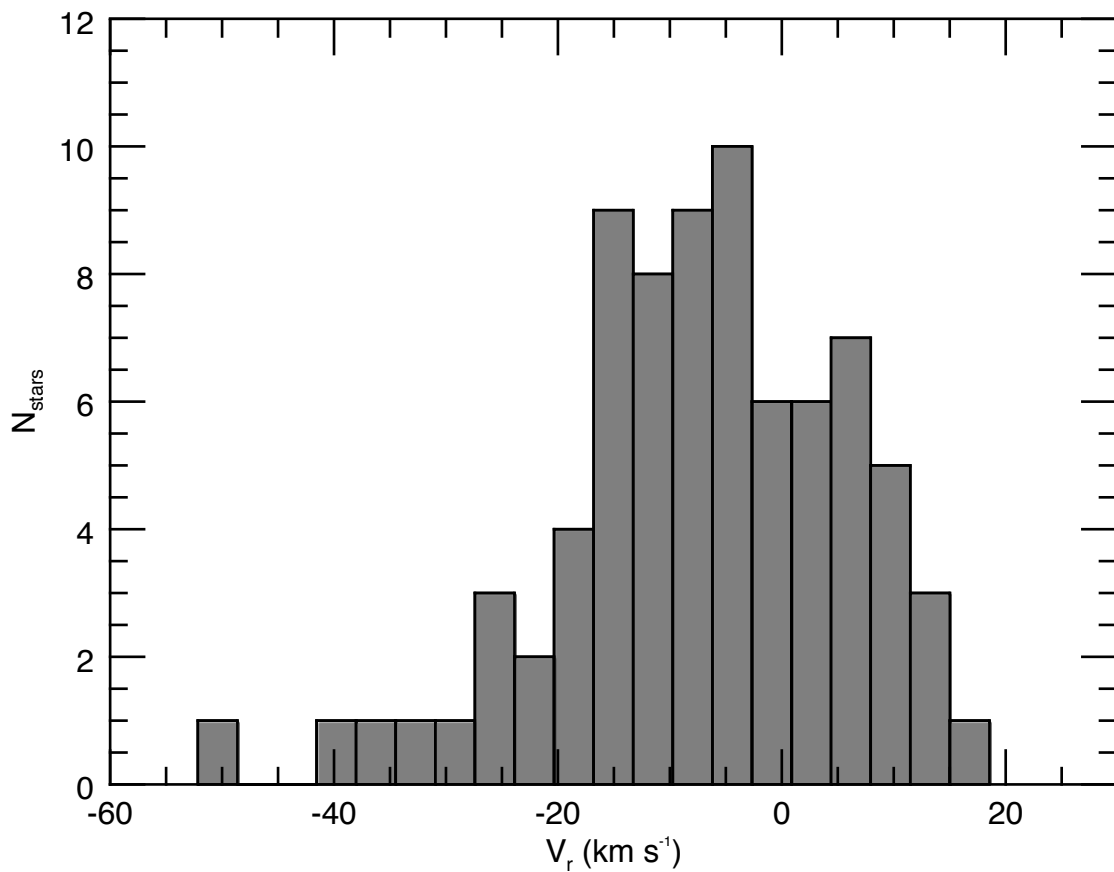


Figure 4. Distribution of radial velocities of the observed stars. Stars that are known or candidate binaries are not included.

et al. 2016). Those authors conclude that higher velocity gas is associated with more distant regions of the Sagittarius-Carina arm of our Galaxy.

Looking at the V_r distribution in Figure 4, we can imagine that the stars with $V_r > 0$ km s $^{-1}$ form a more distant component behind Carina, as suggested by Rebolledo et al. (2016). Using the measured luminosities of the stars that are not in known or candidate binary systems, and the available data on the apparent magnitudes and A_V , we can estimate the distances to these stars. Our results can be found in Table 6. The bolometric corrections (BC) in column 4 are interpolated

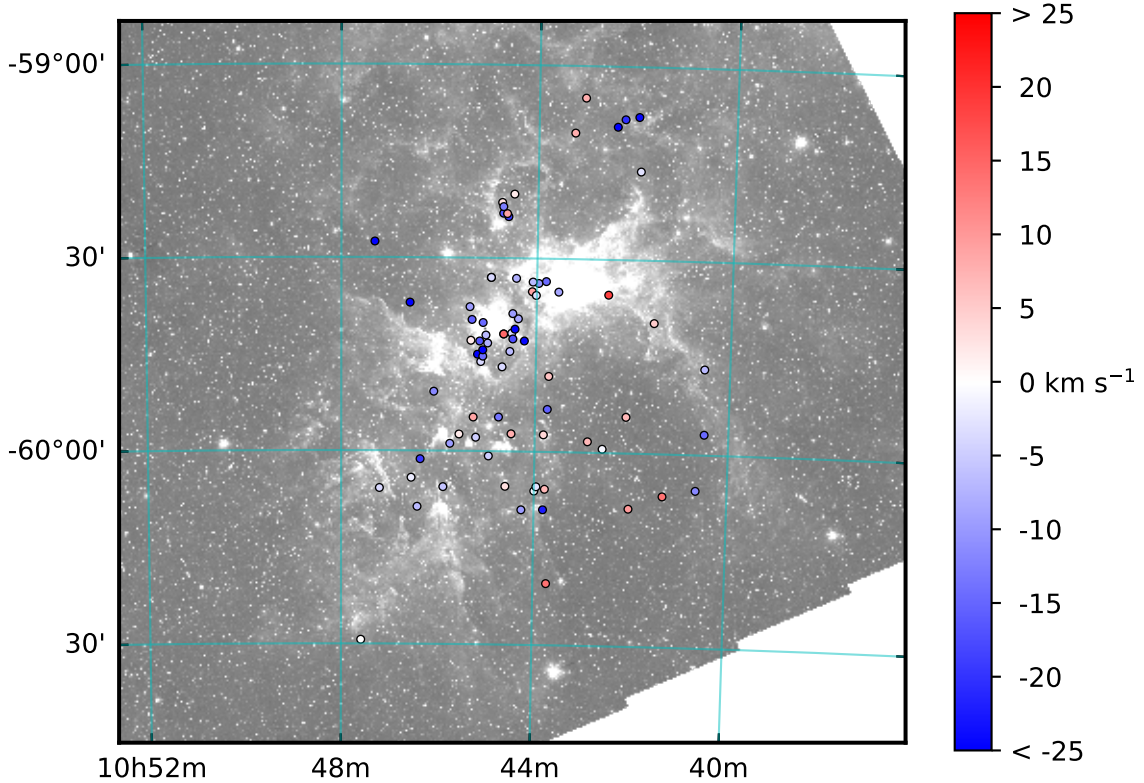


Figure 5. Radial velocity distribution of unpaired stars throughout Carina. The color bar on the right corresponds to the radial velocities of the stars.

from Flower (1996) and Torres (2010). The visible apparent magnitudes (m_V) in column 8 are from the SIMBAD database unless otherwise marked, with assumed uncertainty of 0.1, and the A_V values in column 9 come from Povich et al. (2011). The distances in Table 6 have large uncertainties, and we expect that Gaia parallaxes will resolve the distance uncertainties. In Figure 6, we plot the derived distances against our measured V_r . We find that there is no particular trend between the two quantities, suggesting that the stars with $V_r > 0 \text{ km s}^{-1}$ may not be background stars. The stars LS 1763 and Tr 16-26 could be background stars, with $d > 6,000 \text{ pc}$; however the large uncertainties in their derived distances makes it difficult to be certain.

We find a large degree of V_r dispersion, even in the OB populations associated with Tr 14, Tr 15, and Tr 16, so we estimated the dispersion we might expect for these massive clusters. We assumed the clusters are virialized and tested cluster masses of $1,000 M_\odot$ or $10,000 M_\odot$, and half-radii of 1 pc

or 0.3 pc. This gives a range of V_r dispersions from $\sim 2 \text{ km s}^{-1}$ to $\sim 10 \text{ km s}^{-1}$. The upper part of this range is consistent with our observed dispersion, and it is quite possible that the Carina clusters are not in virial equilibrium, which would increase the expected V_r dispersion. To check the status of virial equilibrium, we estimated the relaxation time of the individual clusters. We assumed that there are about 1,000 to 2,000 stars in the individual Carina clusters and that the stars have velocities within the clusters of around 1 to 10 km s^{-1} . We also assumed the clusters had radii ranging from 1 to 2 pc. The relaxation time for these modeled clusters range from ~ 1.4 to ~ 52 Myr. We know that the clusters like Tr 14 and Tr 16 are about 10 Myr in age (Getman et al. 2014), so it is likely that these clusters are not relaxed, further bolstering the likelihood that they are not yet virialized.

5. SUMMARY

Our goal with this paper was to create a catalog of spectroscopic parameters of a large sample of stars scattered throughout the Carina Nebula. Of the 128 B-type stars we spectroscopically classified in Alexander et al. (2016), 82 of them had a S/N high enough to measure T_{eff} , $\log g$, $V \sin i$, V_r , M_\star , τ_\star , R_\star , and L_{bol} . With the recent and future public data releases from the Gaia-ESO Survey in mind, we also included the radial velocities of the B- and O-type stars in our sample, finding that about 29.2% of our sample are SB1 candidates. We do not find any relationship between distance and V_r , implying that the high V_r stars are probably not a collection of background stars viewed along the tangent of the Sagittarius-Carina arm of the Galaxy. Instead, we conclude that the Carina Nebula has not yet virialized.

The authors would like to thank the referee for several helpful comments that improved this manuscript. The authors would like to thank Sara Martell, Angel Lopez-Sanchez, and Iraklis Konstantopoulos for their assistance with the AAT observations. M.V.M. is supported by the National Science Foundation under grant AST-1109247 and a Class of 1961 Professorship from Lehigh University. R.J.H. and M.V.M. have also received institutional support from Lehigh University. MSP is grateful to the NSF for support from awards AST-1411851 and CAREER-1454333. This research

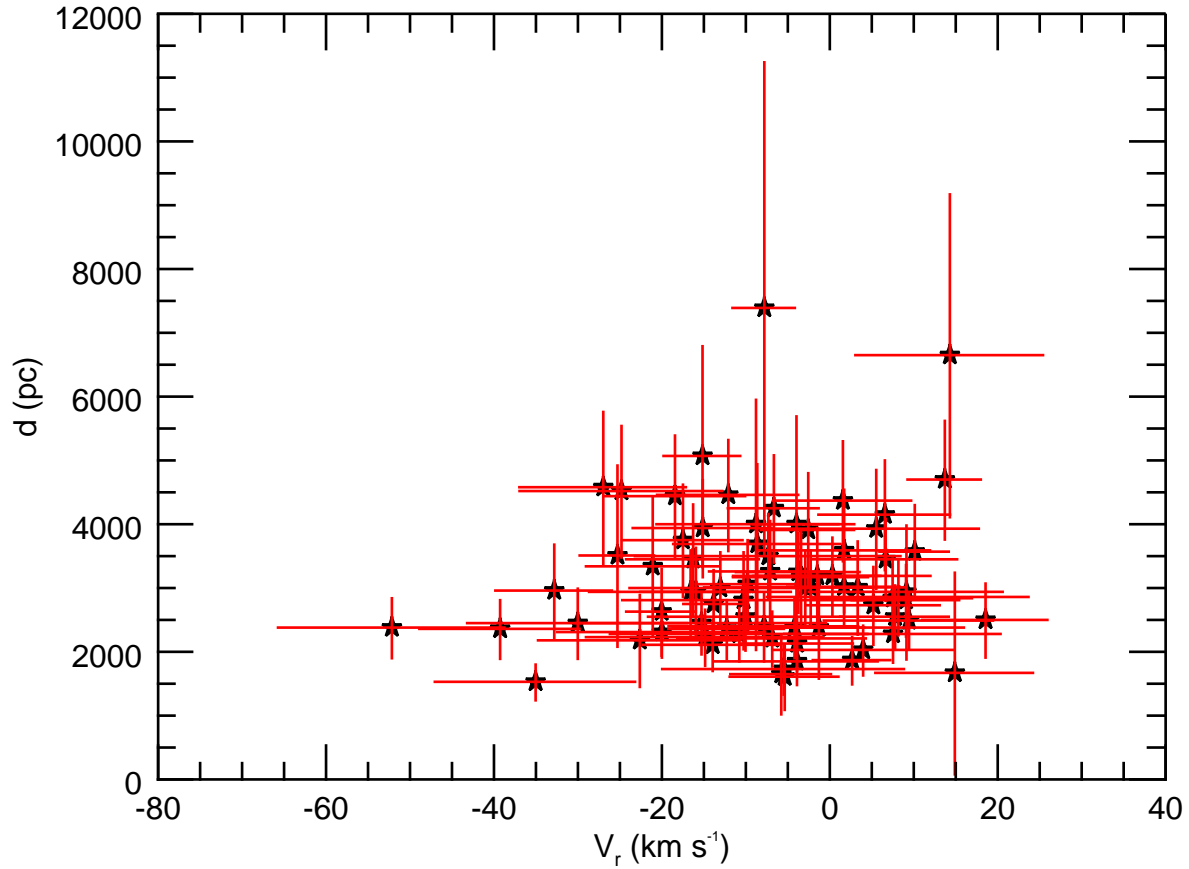


Figure 6. Derived distances vs. radial velocities of the stars not in known or candidate binaries.

has made use of the WEBDA database, operated at the Department of Theoretical Physics and Astrophysics of the Masaryk University and the SIMBAD database, operated at CDS, Strasbourg, France.

Table 1. Projected Rotational Velocities

ID	S/N ₁₃	S/N ₁₄	$V \sin i_{4026}$ ($km s^{-1}$)	$\Delta V \sin i$ ($km s^{-1}$)	$V \sin i_{4388}$ ($km s^{-1}$)	$\Delta V \sin i$ ($km s^{-1}$)	$V \sin i_{4471}$ ($km s^{-1}$)	$\Delta V \sin i$ ($km s^{-1}$)	$V \sin i$ ($km s^{-1}$)	$\Delta V \sin i$ ($km s^{-1}$)
HD 93620	88	104	60	5	65	5	65	5	63	9
HD 305606	63	122	55	5	45	5	50	5	50	9

Table 1 continued on next page

Table 1 (continued)

ID	S/N ₁₃	S/N ₁₄	$V \sin i_{4026}$ ($km\ s^{-1}$)	$\Delta V \sin i$ ($km\ s^{-1}$)	$V \sin i_{4388}$ ($km\ s^{-1}$)	$\Delta V \sin i$ ($km\ s^{-1}$)	$V \sin i_{4471}$ ($km\ s^{-1}$)	$\Delta V \sin i$ ($km\ s^{-1}$)	$V \sin i$ ($km\ s^{-1}$)	$\Delta V \sin i$ ($km\ s^{-1}$)
OBc89	62	113	35	5	35	5	35	5	35	9
HD 93576	74	162	110	10	140	5	135	5	132	12
HD 93501	89	135	185	7	225	7	220	7	210	12
ERO 39	90	174	145	12	160	5	145	5	151	14
OBc75	34	117	45	5	25	5	30	5	33	9
Coll 228-81	56	127	90	5	90	5	100	5	93	9
HD 305538	67	130	90	17	95	10	95	10	94	22
HD 305528	82	130	70	7	65	5	67	9
HD 305533	75	112	205	10	215	15	210	12	209	22
LS 1866	51	138	60	10	60	5	60	5	60	12
LS 1837	76	131	145	10	135	10	140	10	140	17
HD 93097	107	123	185	7	190	7	200	7	192	12
Coll 228-68	97	146	155	7	150	7	160	10	154	14
Coll 228-48	80	126	170	5	175	5	173	7
HD 93027	105	161	80	5	85	5	70	5	78	9
Tr 16-20	95	115	55	7	80	10	50	5	58	13
HD 305521	85	149	95	5	95	5	95	7	95	10
HD 305452	79	172	35	5	35	5	40	5	37	9
LS 1763	44	94	250	15	260	7	265	15	259	22
HD 305535	133	134	175	10	200	5	200	5	195	12
Coll 228-30	52	144	80	10	85	5	90	5	86	12
LS 1813	76	145	95	10	80	5	80	10	84	15
LS 1745	82	180	70	10	75	5	75	5	74	12
LS 1760	50	144	35	5	45	5	45	5	42	9
HD 92877	142	198	115	5	115	5	120	5	117	9
Tr 16-16	72	123	100	12	130	10	135	10	123	19
HD 305437	109	173	105	5	85	5	80	7	91	10
HD 305443	48	145	45	7	30	2	30	2	32	8
HD 305518	81	146	100	7	130	5	105	10	115	13

Table 1 continued on next page

Table 1 (*continued*)

ID	S/N ₁₃	S/N ₁₄	$V \sin i_{4026}$	$\Delta V \sin i$	$V \sin i_{4388}$	$\Delta V \sin i$	$V \sin i_{4471}$	$\Delta V \sin i$	$V \sin i$	$\Delta V \sin i$
			($km\ s^{-1}$)	($km\ s^{-1}$)	($km\ s^{-1}$)	($km\ s^{-1}$)	($km\ s^{-1}$)	($km\ s^{-1}$)	($km\ s^{-1}$)	($km\ s^{-1}$)
HD 92644	106	179	185	7	190	7	195	10	189	14
Tr 16-17	59	133	240	12	235	10	245	12	240	20
HD 303225	85	162	75	10	80	7	85	7	81	14
Tr 16-11	103	95	305	10	305	15	305	18
HD 92937	108	191	115	7	145	5	130	7	132	11
Tr 16-94	120	153	125	20	120	5	130	5	125	21
Tr 14-30	50	138	50	5	55	5	50	5	52	9
Tr 14-27	33	120	75	17	70	7	70	5	71	19
HD 303189	69	131	95	10	100	5	100	7	99	13
HD 303202	64	135	140	7	165	5	170	10	158	13
HD 303297	71	151	60	5	60	5	50	5	57	9
HD 92894	88	180	75	5	80	5	75	7	77	10
HD 303296	86	139	75	5	80	5	65	5	73	9
Tr 15-23	42	98	45	10	50	5	40	5	45	12
HD 93026	86	150	95	5	105	5	95	7	99	10
HD 93002	83	154	70	5	70	5	65	7	69	10
LS 1822	73	107	60	12	75	7	65	5	67	15
Tr 16-122	29	103	115	5	125	5	120	7
Tr 14-19	28	77	240	10	240	10
Tr 15-15	...	117	140	10	130	10	135	14
HD 93249 A	...	130	110	5	110	5
Tr 15-26	47	102	35	5	40	5	35	5	37	9
Tr 16-31	70	106	225	12	225	7	210	7	219	16
Tr 16-124	22	102	95	7	105	7	100	10
Tr 16-4	37	88	70	17	100	5	100	5	96	18
HD 303402	46	122	110	5	115	10	112	11
Tr 16-2	48	99	250	17	220	12	245	7	239	20
HD 93723	122	186	55	5	40	5	40	5	45	9
Tr 16-3	70	134	65	5	55	5	60	7

Table 1 continued on next page

Table 1 (*continued*)

ID	S/N ₁₃	S/N ₁₄	$V \sin i_{4026}$	$\Delta V \sin i$	$V \sin i_{4388}$	$\Delta V \sin i$	$V \sin i_{4471}$	$\Delta V \sin i$	$V \sin i$	$\Delta V \sin i$
			($km\ s^{-1}$)	($km\ s^{-1}$)	($km\ s^{-1}$)	($km\ s^{-1}$)	($km\ s^{-1}$)	($km\ s^{-1}$)	($km\ s^{-1}$)	($km\ s^{-1}$)
Tr 16-115	81	128	150	5	140	5	125	5	138	9
OBc68	61	202	20	7	20	5	25	5	22	10
OBc60	9	88	80	5	80	5	80	7
OBc57	51	267	60	15	65	5	60	5	62	17
OBc23	114	244	60	12	75	5	65	5	68	14
Tr 16-246	...	171	135	7	135	7	135	10
Tr 14-18	30	166	125	5	145	5	135	7
Tr 14-28	15	159	80	30	55	7	60	31
Tr 14-22	...	128	345	10	345	10
Tr 15-19	18	134	215	7	235	5	227	9
Tr 16-18	58	155	80	5	115	7	95	9
Tr 14-29	31	186	180	12	125	10	165	15	154	22
Tr 16-12	31	190	55	5	100	20	64	21
Tr 15-21	12	126	290	15	290	7	290	17
Tr 16-14	42	181	90	5	90	5
Tr 15-9	33	118	180	5	170	5	175	7
Tr 16-25	...	156	45	5	55	5	50	7
Tr 16-28	42	179	40	10	45	5	55	5	48	12
Tr 16-55	4	152	115	5	145	5	130	7
Tr 16-24	10	159	205	5	225	10	212	11
Tr 16-74	47	160	105	7	100	5	110	5	105	10
Tr 16-26	59	...	195	37	195	37

Table 2. Physical Parameters

ID	T_{eff}	ΔT_{eff}	$\log g$	$\Delta \log g$	τ_{\star}	$\Delta \tau_{\star}$	M_{\star}	ΔM_{\star}	R_{\star}	ΔR_{\star}	L_{bol}	ΔL_{bol}
	(K)	(K)	(dex)	(dex)	(Myr)	(Myr)	(M_{\odot})	(M_{\odot})	(R_{\odot})	(R_{\odot})	(L_{\odot})	(L_{\odot})
HD 93620	19800	650	3.3	0.11	16.43	5.19	11.7	1.97	12.67	2.69	22160	9850

Table 2 continued on next page

Table 2 (*continued*)

ID	T_{eff}	ΔT_{eff}	$\log g$	$\Delta \log g$	τ_{\star}	$\Delta \tau_{\star}$	M_{\star}	ΔM_{\star}	R_{\star}	ΔR_{\star}	L_{bol}	ΔL_{bol}
	(K)	(K)	(dex)	(dex)	(Myr)	(Myr)	(M_{\odot})	(M_{\odot})	(R_{\odot})	(R_{\odot})	(L_{\odot})	(L_{\odot})
HD 305606	21100	550	4.11	0.11	19.7	7.48	7.64	0.73	4.03	0.71	2890	1060
OBc89	17700	650	3.26	0.12	22.8	8.13	10	1.8	12.27	2.82	13270	6410
HD 93576	28700	350	3.72	0.11	7.65	0.85	18.07	2.46	9.71	1.9	57460	22700
HD 93501	29700	350	3.87	0.1	7.26	0.3	17.15	1.9	7.96	1.36	44280	15330
ERO 39	26700	2000	3.63	0.22	9.04	3.99	16.65	7.2	10.34	4.97	48780	49190
OBc75	29700	350	3.89	0.13	7.25	0.45	16.87	2.25	7.72	1.68	41590	18250
Coll 228-81	27000	1000	4.38	0.22	0	3.78	10.31	2.36	3.43	1.28	5620	4270
HD 305538	25500	1350	4.27	0.16	2.52	6.1	10.13	1.87	3.86	1.07	5660	3370
HD 305528	15000	300	3.3	0.11	40.66	12.37	7.21	0.96	9.95	1.94	4500	1790
HD 305533	29400	650	4.11	0.14	5.62	3.14	14.24	1.72	5.5	1.23	20310	9290
LS 1866	27200	1000	4.35	0.18	0	3.46	10.74	2.13	3.63	1.12	6460	4110
LS 1837	26300	900	4.09	0.16	9.2	4.91	11.46	1.64	5.05	1.31	10960	5890
HD 93097	26800	200	3.75	0.11	9.62	0.85	14.82	1.73	8.5	1.58	33440	12530
Coll 228-68	27100	1000	4.15	0.2	6.51	5.49	11.8	2.11	4.78	1.56	11080	7400
Coll 228-48	19000	1150	4.12	0.18	29.7	19.38	6.41	1.17	3.65	1.1	1560	1020
HD 93027	29700	300	3.66	0.11	6.46	0.82	20.82	3.04	11.17	2.25	87180	35250
Tr 16-20	18200	600	3.63	0.13	37.86	6.84	7.55	0.98	6.96	1.51	4780	2170
HD 305521	29500	600	4.12	0.12	5.34	2.85	14.27	1.47	5.45	1.04	20170	7890
HD 305452	20900	500	3.36	0.11	15.16	4.27	12.18	1.82	12.07	2.45	24950	10410
LS 1763	22100	1250	3.42	0.18	14.21	6.56	12.8	3.71	11.55	4.14	28560	21490
HD 305535	15000	500	3.15	0.11	31.56	9.28	8.36	1.41	12.74	2.7	7370	3280
Coll 228-30	21200	750	3.82	0.13	23.18	3.81	8.95	1.36	6.09	1.39	6730	3220
LS 1813	23200	800	3.84	0.13	17.46	2.81	10.52	1.62	6.46	1.47	10840	5170
LS 1745	22800	550	3.57	0.11	16.27	2.59	11.74	1.37	9.30	1.74	21000	8130
LS 1760	28600	400	3.63	0.11	7.13	1.03	19.44	3.01	11.17	2.30	74980	31150
HD 92877	21800	650	3.65	0.11	18.97	3.24	10.76	1.2	8.12	1.48	13380	5140
Tr 16-16	28000	1500	4.30	0.18	0.58	63.56	11.77	19.04	4.02	3.81	8920	17010
HD 305437	29500	550	3.95	0.11	7.24	0.97	15.79	1.97	6.97	1.33	33000	12820
HD 305443	22100	650	3.65	0.11	17.98	3.22	11.02	1.21	8.22	1.49	14480	5530

Table 2 continued on next page

Table 2 (*continued*)

ID	T_{eff}	ΔT_{eff}	$\log g$	$\Delta \log g$	τ_{\star}	$\Delta \tau_{\star}$	M_{\star}	ΔM_{\star}	R_{\star}	ΔR_{\star}	L_{bol}	ΔL_{bol}
	(K)	(K)	(dex)	(dex)	(Myr)	(Myr)	(M_{\odot})	(M_{\odot})	(R_{\odot})	(R_{\odot})	(L_{\odot})	(L_{\odot})
HD 305518	26600	400	3.25	0.11	6.63	1.3	23.39	4.98	18.98	4.45	161970	76690
HD 92644	29800	150	3.71	0.11	6.6	0.63	19.78	2.53	10.28	1.98	74800	28830
Tr 16-17	28200	1700	3.82	0.2	8.48	1.85	15.78	5.15	8.09	3.25	37150	31200
HD 303225	21300	1000	3.62	0.11	21.26	4.93	10.31	1.52	8.23	1.66	12530	5570
Tr 16-11	23000	1500	3.74	0.27	16.83	5.34	11.09	3.23	7.44	3.49	13890	13560
HD 92937	17700	700	3.20	0.11	20.44	6.85	10.63	1.94	13.56	2.97	16190	7550
Tr 16-94	23200	600	4.10	0.11	14.28	5.5	8.98	0.88	4.42	0.78	5080	1880
Tr 14-30	26100	1300	3.24	0.11	6.88	2.44	22.62	8.97	18.89	6.1	148600	100500
Tr 14-27	28600	1000	4.60	0.13	0.00	0.00	9.30	1.76	2.53	0.62	3850	1970
HD 303189	21400	800	3.45	0.11	16.44	5.25	11.69	2.00	10.66	2.28	21400	9700
HD 303202	23100	850	3.52	0.12	13.94	3.21	12.91	1.99	10.33	2.24	27300	12520
HD 303297	27800	2000	4.02	0.22	8.43	4.78	13.28	3.92	5.9	2.43	18640	16270
HD 92894	25800	1250	3.55	0.16	9.41	2.69	16.62	4.00	11.33	3.48	51050	32950
HD 303296	24300	750	3.67	0.13	12.79	2.96	13.01	2.24	8.73	2.08	23860	11740
Tr 15-23	23500	750	4.07	0.13	14.71	5.53	9.36	1.15	4.67	1.00	5980	2660
HD 93026	23700	650	3.9	0.11	16.41	1.8	10.52	1.25	6.02	1.13	10280	4010
HD 93002	22900	750	3.65	0.11	15.42	3.3	11.71	1.6	8.47	1.66	17730	7330
LS 1822	29800	150	4.07	0.11	5.96	1.74	14.86	1.09	5.89	0.97	24530	8120
Tr 16-122	23200	1000	4.10	0.12	14.28	6.74	8.98	1.21	4.42	0.92	5080	2280
Tr 14-19	15300	1000	3.5	0.14	58.5	26.4	6.31	1.41	7.39	2.04	2690	1640
Tr 15-15	23000	850	3.45	0.11	13.27	3.88	13.41	2.48	11.42	2.52	32760	15240
HD 93249 A	26800	250	3.26	0.1	6.59	1.35	23.51	5.93	18.82	4.55	163970	79660
Tr 15-26	23700	900	3.75	0.14	14.96	3.56	11.59	2.10	7.51	1.91	15990	8500
Tr 16-31	29600	450	3.89	0.11	7.33	0.5	16.73	2.11	7.68	1.47	40700	15730
Tr 16-124	29500	600	4.02	0.22	6.73	3.02	14.94	2.84	6.25	2.24	26580	19200
Tr 16-4	29700	400	4.13	0.16	4.98	3.38	14.4	1.66	5.41	1.32	20440	10080
HD 303402	21700	850	3.29	0.12	12.3	3.78	14.05	2.98	14.05	3.46	39310	20330
Tr 16-2	29500	650	4.1	0.16	5.73	3.29	14.39	1.97	5.60	1.43	21290	11080
HD 93723	17800	300	3.73	0.11	38.62	4.07	7.12	0.5	6.03	0.98	3270	1080

Table 2 continued on next page

Table 2 (*continued*)

ID	T_{eff}	ΔT_{eff}	$\log g$	$\Delta \log g$	τ_{\star}	$\Delta \tau_{\star}$	M_{\star}	ΔM_{\star}	R_{\star}	ΔR_{\star}	L_{bol}	ΔL_{bol}
	(K)	(K)	(dex)	(dex)	(Myr)	(Myr)	(M_{\odot})	(M_{\odot})	(R_{\odot})	(R_{\odot})	(L_{\odot})	(L_{\odot})
Tr 16-3	29700	350	3.78	0.11	7.05	0.63	18.5	2.45	9.17	1.78	58770	23000
Tr 16-115	29800	250	3.57	0.11	5.9	0.77	23.37	4.05	13.13	2.82	122020	52620
OBc68	29100	1000	4.37	0.16	0.00	1.81	11.89	2.36	3.73	1.07	8950	5270
OBc60	25100	950	3.86	0.16	12.68	2.13	11.9	2.22	6.71	1.89	16030	9350
OBc57	21800	850	4.17	0.14	14.2	10.73	7.9	0.99	3.82	0.86	2970	1420
OBc23	16600	700	3.44	0.13	38.12	15.65	7.52	1.35	8.65	2.09	5100	2610
Tr 16-246	28100	2000	3.87	0.18	8.58	2.12	14.9	4.69	7.42	2.75	30820	24520
Tr 14-18	22600	650	4.1	0.11	15.91	6.12	8.62	0.86	4.33	0.77	4390	1640
Tr 14-28	28900	1000	4.24	0.16	2.19	3.73	13.05	2.05	4.54	1.2	12890	7040
Tr 14-22	20800	1350	3.53	0.16	21.28	7.89	10.4	2.5	9.17	2.83	14130	9480
Tr 15-19	16000	750	3.83	0.14	62.94	12.75	5.74	0.87	4.82	1.15	1370	700
Tr 16-18	29500	650	4.26	0.13	1.35	2.81	13.5	1.65	4.51	0.95	13810	5950
Tr 14-29	23100	1050	4.14	0.14	12.84	8.83	8.79	1.27	4.18	0.99	4460	2260
Tr 16-12	29500	650	4.12	0.14	5.34	3.22	14.27	1.71	5.45	1.22	20170	9200
Tr 15-21	15200	200	3.92	0.11	74.13	4.75	4.96	0.44	4.04	0.7	780	270
Tr 16-14	27000	2000	4.11	0.18	7.68	6.32	11.89	2.87	5.03	1.68	12060	8810
Tr 15-9	17400	500	3.85	0.11	47.55	7.84	6.44	0.68	4.99	0.9	2050	780
Tr 16-25	20100	500	4.05	0.14	25.67	5.63	7.2	0.54	4.19	0.84	2580	1030
Tr 16-28	29200	400	4.36	0.12	0.00	1.11	12.07	1.54	3.8	0.77	9420	3870
Tr 16-55	25000	1100	4.15	0.14	9.28	6.93	10.22	1.45	4.45	1.04	6950	3480
Tr 16-24	22300	800	4.1	0.13	16.75	7.62	8.43	1.03	4.28	0.91	4070	1830
Tr 16-74	29300	850	4.22	0.13	2.72	3.40	13.55	1.74	4.73	1.01	14800	6580
Tr 16-26	24800	2000	3.44	0.22	10.19	4.98	16.11	7.19	12.66	6.18	54430	56050

Table 3. Radial Velocity Measurements of B-type stars

ID	$V_{r,2013}$	$\Delta V_{r,2013}$	$V_{r,2014}$	$\Delta V_{r,2014}$	Notes
	km s ⁻¹	km s ⁻¹	km s ⁻¹	km s ⁻¹	
HD 93620	21.18	4.69	-38.98	1.96	SB1c
HD 305606	12.99	5.43	-16.53	3.58	SB1c
OBe89	6.68	1.51	-11.30	2.42	SB1c
HD 93576	7.90	6.38	-73.85	13.35	SB1c , SB ^b
HD 93501	-23.51	9.09	-16.49	8.50	...
ERO 39	1.00	6.73	53.81	9.70	SB1c
OBe75	8.65	5.59	-8.80	3.57	...
Coll 228-81	2.91	4.42	-14.46	4.16	...
HD 305538	23.84	6.13	-47.87	8.99	SB1c , Double/Multiple Star ^b
HD 305528	19.61	6.18	-1.44	1.94	...
HD 305533	4.91	2.89	-15.88	14.18	...
LS 1866	4.15	1.36	-14.88	6.41	...
LS 1837	0.30	9.13	-20.83	11.19	...
HD 93097	17.07	7.79	-3.77	3.80	...
Coll 228-68	9.32	17.23	-11.91	2.59	...
Coll 228-48	-13.76	5.62	-31.50	10.73	...
HD 93027	10.26	2.16	-12.01	4.13	SB1c
Tr 16-20	10.83	4.82	-21.31	3.58	SB1c
HD 305521	12.41	6.38	-4.48	8.74	...
HD 305452	7.83	2.69	12.41	3.22	...
LS 1763	15.61	10.17	12.99	4.82	...
HD 305535	13.00	6.46	1.95	7.10	...
Coll 228-30	11.26	6.20	-14.23	4.51	...
LS 1813	-9.73	3.38	-22.18	5.66	...
LS 1745	1.38	8.06	-25.55	2.64	...
LS 1760	12.58	6.82	0.53	4.00	...
HD 92877	-2.57	5.28	-25.32	6.38	Double/Multiple Star ^b
Tr 16-16	4.13	3.45	25.66	8.81	...

Table 3 continued on next page

Table 3 (*continued*)

ID	$V_{r,2013}$	$\Delta V_{r,2013}$	$V_{r,2014}$	$\Delta V_{r,2014}$	Notes
	km s ⁻¹	km s ⁻¹	km s ⁻¹	km s ⁻¹	
HD 305437	44.78	11.41	-6.23	5.45	SB1c
HD 305443	-3.42	4.26	-26.84	7.17	...
HD 305518	5.19	6.36	5.87	10.61	...
HD 92644	7.57	6.89	-22.20	14.32	...
Tr 16-17	3.32	4.95	-11.27	1.42	...
HD 303225	16.34	7.04	-5.96	3.91	...
Tr 16-11	-11.39	9.05	-6.19	7.65	...
HD 92937	32.95	4.36	4.15	6.13	...
Tr 16-94	-28.43	10.05	-41.64	6.56	...
Tr 14-30	-5.24	9.86	-12.04	1.73	...
Tr 14-27	8.20	5.10	-19.34	3.27	SB1c
HD 303189	-16.96	10.16	-32.66	6.65	...
HD 303202	-2.57	5.61	...
HD 303297	-4.68	3.83	-60.11	1.22	SB1c
HD 92894	-14.83	7.55	-27.35	2.47	...
HD 303296	-34.34	6.69	-31.31	2.11	...
Tr 15-23	11.47	2.95	-7.86	2.85	SB1c
HD 93026	17.47	12.31	-2.40	4.06	...
HD 93002	21.83	10.39	-5.48	11.70	...
LS 1822	21.93	13.59	-46.34	3.33	SB1c
Tr 16-122	3.91	8.40	-19.56	7.67	...
Tr 14-19	10.24	0.66	-3.46	0.85	SB1c
Tr 15-15	-17.49	7.25	...
HD 93249 A	3.32	1.77	...
Tr 15-26	12.54	9.91	-9.12	3.03	...
Tr 16-31	11.62	11.72	-11.01	1.63	...
Tr 16-124	18.23	9.40	0.03	6.81	...
Tr 16-4	3.33	5.53	-17.55	4.72	...
HD 303402	-13.40	6.87	-40.56	7.25	...

Table 3 continued on next page

Table 3 (*continued*)

ID	$V_{r,2013}$	$\Delta V_{r,2013}$	$V_{r,2014}$	$\Delta V_{r,2014}$	Notes
	km s ⁻¹	km s ⁻¹	km s ⁻¹	km s ⁻¹	
Tr 16-2	15.10	2.82	-6.62	1.00	SB1c
HD 93723	14.55	4.29	-17.17	3.71	SB1c
Tr 16-3	5.20	5.64	-12.67	4.86	...
Tr 16-115	16.13	5.03	-13.00	6.58	...
OBc68	-2.90	7.15	-36.22	2.01	SB1c
OBc60	2.45	4.12	-22.84	5.71	...
OBc57	-5.48	1.24	-22.89	1.24	SB1c
OBc23	11.61	2.88	-13.10	2.32	SB1c
Tr 16-246	-25.29	4.50	...
Tr 14-18	0.21	15.14	-21.76	2.86	...
Tr 14-28	25.73	7.25	-18.06	2.05	SB1c
Tr 14-22	-15.16	4.64	...
Tr 15-19	-22.81	3.74	-17.26	1.96	...
Tr 16-18	-9.51	4.28	-27.37	7.36	...
Tr 14-29	-7.69	5.43	-6.02	4.94	ERO 21 ^c
Tr 16-12	-1.22	3.64	-18.35	4.99	...
Tr 15-21	27.71	5.41	-8.84	8.59	...
Tr 16-14	28.26	6.47	-8.85	1.16	SB1c
Tr 15-9	-6.58	8.59	-19.51	6.56	...
Tr 16-25	-30.55	4.81	SB2c ^a
Tr 16-28	3.84	11.23	-23.92	2.94	...
Tr 16-55	-11.13	6.85	-21.44	4.10	...
Tr 16-24	-28.27	9.73	-31.76	8.87	...
Tr 16-74	-8.92	6.94	-24.24	9.91	...
Tr 16-26	-7.80	3.79

^aSee Section 3 for details^bSimbad^cSexton et al. 2015

Table 4. Radial Velocity Measurements of O-type stars

ID	$V_{r,2013}$	$\Delta V_{r,2013}$	$V_{r,2014}$	$\Delta V_{r,2014}$	Notes
	km s ⁻¹	km s ⁻¹	km s ⁻¹	km s ⁻¹	
Tr 16-127	5.39	6.44	-12.22	4.93	...
HD 305438	4.23	2.85	-12.95	1.67	SB1c
HD 303316	16.58	2.66	-7.67	0.89	SB1c
HD 93028	31.53	2.52	23.83	2.06	SB ^a
HD 303312	-0.24	0.81	EB ^a
HD 305556	22.48	3.77	4.93	2.34	...
Tr 14-21	-6.09	5.50	SB ^b
HD 93128	24.56	6.18	-11.44	4.09	SB1c, SB ^c
LS 1821	11.56	8.54	-17.40	8.51	...
HD 93130	-71.22	8.26	-50.85	1.96	EB ^a
HD 305536	20.32	4.97	13.20	3.01	SB ^a
HD 305523	19.51	5.85	-3.96	2.92	...
HD 93204	-1.71	8.45	-12.02	7.50	...
HD 93222	12.10	4.10	-6.79	2.26	...
HD 303311	29.86	1.14	-15.21	8.17	SB1c, Double/Multiple Star ^a
Tr 16-100	-8.70	8.43	0.87	4.92	...
HD 305524	-14.16	3.34	-13.52	1.32	...
LS 1865	15.13	4.70	-14.35	3.76	SB1c
Tr 16-23	-10.80	9.95	-18.90	10.11	...
HD 303308	-11.90	14.55	-18.65	3.55	...
Tr 16-22	5.87	5.47	-13.66	4.04	...
HD 93343	-45.61	9.27	-58.72	9.90	...
HD 305532	8.43	5.88	-5.04	3.34	...
FO 15	-0.37	3.68	-102.87	6.22	SB1c, EB ^a
HD 305525	-9.44	5.24	-15.11	4.56	...
LS 1892	0.58	1.12	-18.91	1.32	SB1c
LS 1893	1.43	4.70	-14.76	2.83	...
HD 305539	8.32	6.96	-12.88	2.97	...

Table 4 continued on next page

Table 4 (*continued*)

ID	$V_{r,2013}$	$\Delta V_{r,2013}$	$V_{r,2014}$	$\Delta V_{r,2014}$	Notes
	km s ⁻¹	km s ⁻¹	km s ⁻¹	km s ⁻¹	
HD 303304	-40.47	1.71	-38.07	9.45	...
HD 93632	2.79	7.24	-11.20	4.36	...
LS 1914	13.91	6.39	-9.07	0.37	SB1c
HD 305619	5.87	4.04	-16.81	3.17	SB1c
HD 305599	28.09	7.61	-10.35	2.96	SB1c

NOTE—EB - eclipsing binary; SB - spectroscopic binary

^aSimbad

^bWEBDA

^cLevato et al. 1991

Table 5. Radial Velocity Measurements of SB2s

ID	$V_{r,p,2013}$	$\Delta V_{r,p,2013}$	$V_{r,p,2014}$	$\Delta V_{r,p,2014}$	$V_{r,s,2013}$	$\Delta V_{r,s,2013}$	$V_{r,s,2014}$	$\Delta V_{r,s,2014}$
	km s ⁻¹	km s ⁻¹	km s ⁻¹	km s ⁻¹	km s ⁻¹	km s ⁻¹	km s ⁻¹	km s ⁻¹
HD 303313	-120.32	9.94	-69.32	8.88	125.76	13.22	34.82	4.04
HD 93056	14.08	4.27	-96.40	10.81	85.60	8.56
HD 305522	23.28	9.32	52.60	5.23	-31.70	13.86	-67.47	3.17
LS 1840	-16.51	7.29	-14.19	8.83	44.88	12.22
HD 305534	-142.93	10.71	-117.25	19.91	145.33	33.07	96.26	31.15
Tr 16-9	22.09	2.24	-77.82	7.78	-31.48	6.44	66.80	2.52
Tr 16-1	-44.65	3.08	-129.93	12.48	37.23	0.67	86.52	22.96
OBc49	-48.48	11.55	-83.57	9.72	86.70	22.22	45.22	12.78
HD 92607	-185.04	10.79	-38.16	9.23	206.76	23.44	20.98	8.91
Tr 16-10	29.77	7.21	-14.26	8.35
Tr 16-21	44.01	10.91	99.07	3.99	-58.98	10.60	-87.22	2.23

Table 6. Photometry and Derived Distances

ID	M_{bol}	ΔM_{bol}	BC	ΔBC	M_V	ΔM_V	V	A_V	d (pc)	Δd (pc)
(1)	(2)	(3)	(4)	(5)	(6)	(7)	(8)	(9)	(10)	(11)
Coll 228-30	-4.84	1.20	-2.02	0.18	-2.82	1.21	10.8 ^a	1.10	3190	770
Coll 228-48	-3.25	1.63	-1.78	0.31	-1.47	1.66	11.00 ^a	0.78	2180	730
Coll 228-68	-5.38	1.67	-2.61	0.22	-2.77	1.68	10.16 ^a	1.05	2380	800
Coll 228-81	-4.64	1.90	-2.60	0.22	-2.04	1.91	10.89 ^a	1.85	1650	630
HD 303189	-6.10	1.13	-2.04	0.19	-4.05	1.15	10.10	0.88	4520	1040
HD 303202	-6.36	1.15	-2.22	0.20	-4.14	1.16	9.80	0.98	3910	910
HD 303225	-5.51	1.11	-2.03	0.24	-3.48	1.14	9.74	1.04	2730	620
HD 303296	-6.21	1.23	-2.34	0.17	-3.88	1.24	9.50	1.02	2960	740
HD 303304	-5.00 ^b	0.30 ^b	9.71	2.85	2360	470
HD 303308	-5.50 ^b	0.30 ^b	8.17	1.72	2450	490
HD 303402	-6.76	1.29	-2.07	0.20	-4.68	1.31	10.69	2.07	4580	1200
HD 305443	-5.67	0.95	-2.12	0.15	-3.56	0.97	10.60	1.18	3940	770
HD 305452	-6.26	1.04	-1.99	0.12	-4.27	1.05	9.56	1.07	3570	750
HD 305518	-8.29	1.18	-2.56	0.09	-5.73	1.19	9.72	2.48	3930	940
HD 305521	-6.03	0.98	-2.84	0.13	-3.19	0.99	9.81	1.46	2030	400
HD 305523	-5.50 ^b	0.30 ^b	8.50	1.97	2550	510
HD 305524	-5.00 ^b	0.30 ^b	9.32	2.12	2750	550
HD 305525	-5.50 ^b	0.30 ^b	10.00	3.64	2360	470
HD 305528	-4.40	0.99	-1.24	0.11	-3.16	1.00	10.32	1.24	2810	570
HD 305532	-5.00 ^b	0.30 ^b	10.20	2.80	3020	610
HD 305533	-6.04	1.14	-2.83	0.14	-3.21	1.15	10.32	2.33	1730	400
HD 305535	-4.94	1.11	-1.24	0.18	-3.70	1.13	9.39	0.82	2840	640
HD 305539	-4.65 ^b	0.30 ^b	9.90	2.16	3010	600
HD 305556	-6.00 ^b	0.30 ^b	8.95	1.59	4700	940
HD 92644	-7.45	0.96	-2.87	0.03	-4.58	0.96	8.88	0.74	3500	680
HD 92877	-5.59	0.96	-2.08	0.16	-3.50	0.97	8.50	0.38	2110	410
HD 92894	-7.04	1.61	-2.48	0.28	-4.56	1.64	9.53	1.47	3340	1090
HD 92937	-5.79	1.17	-1.62	0.20	-4.17	1.18	8.95	1.13	2500	590

Table 6 continued on next page

Table 6 (*continued*)

ID	M_{bol}	ΔM_{bol}	BC	ΔBC	M_V	ΔM_V	V	A_V	d (pc)	Δd (pc)
(1)	(2)	(3)	(4)	(5)	(6)	(7)	(8)	(9)	(10)	(11)
HD 93002	-5.89	1.03	-2.20	0.17	-3.69	1.05	9.71	1.12	2860	600
HD 93026	-5.30	0.98	-2.28	0.15	-3.02	0.99	9.67	0.90	2280	450
HD 93097	-6.58	0.94	-2.58	0.04	-4.00	0.94	9.76	1.07	3450	650
HD 93204	-5.00 ^b	0.30 ^b	8.42	1.70	2210	440
HD 93222	-5.00 ^b	0.30 ^b	8.10	1.74	1870	380
HD 93249	-8.31	1.21	-2.58	0.06	-5.73	1.22	8.20	1.53	3010	740
HD 93343	-4.65 ^b	0.30 ^b	9.56	2.33	2380	480
HD 93501	-6.89	0.87	-2.86	0.08	-4.02	0.87	9.09	1.30	2310	400
HD 93632	-5.50 ^b	0.30 ^b	9.10	2.72	2380	480
LS 1745	-6.08	0.97	-2.19	0.13	-3.89	0.98	9.92	0.56	4460	880
LS 1760	-7.46	1.04	-2.76	0.09	-4.70	1.04	10.61	2.22	4150	870
LS 1763	-6.41	1.88	-2.12	0.30	-4.29	1.90	11.18	1.36	6650	2540
LS 1813	-5.36	1.19	-2.23	0.19	-3.13	1.21	10.43	1.22	2940	710
LS 1821	-4.30 ^b	0.30 ^b	9.31	1.22	3010	600
LS 1837	-5.37	1.34	-2.53	0.20	-2.84	1.36	10.52	1.11	2810	770
LS 1866	-4.80	1.59	-2.62	0.22	-2.18	1.61	10.81	1.95	1610	520
LS 1893	-4.00 ^b	0.30 ^b	10.80	1.66	4250	850
OBc60	-5.78	1.46	-2.42	0.21	-3.37	1.47	...	4.90
OBc75	-6.82	1.10	-2.86	0.08	-3.96	1.10	...	2.50
Tr 14-18	-4.38	0.93	-2.17	0.15	-2.21	0.95	11.90	2.32	2280	430
Tr 14-22	-5.65	1.68	-1.98	0.33	-3.67	1.71	12.23	2.37	5070	1740
Tr 14-29	-4.39	1.27	-2.22	0.24	-2.18	1.29	11.94
Tr 14-30	-8.20	1.69	-2.51	0.29	-5.69	1.72	10.07	2.92	3690	1270
Tr 15-15	-6.56	1.16	-2.21	0.20	-4.35	1.18	10.08 ^a	1.56	3750	890
Tr 15-19	-3.11	1.28	-1.39	0.25	-1.72	1.30	12.71 ^a	2.33	2630	690
Tr 15-21	-2.50	0.87	-1.27	0.07	-1.23	0.87	13.13 ^a	2.38	2490	440
Tr 15-26	-5.78	1.33	-2.28	0.21	-3.50	1.34	10.70 ^a	1.43	3590	970
Tr 15-9	-3.55	0.95	-1.58	0.15	-1.97	0.96	12.59 ^a	2.17	3000	580

Table 6 continued on next page

Table 6 (*continued*)

ID	M_{bol}	ΔM_{bol}	BC	ΔBC	M_V	ΔM_V	V	A_V	d (pc)	Δd (pc)
(1)	(2)	(3)	(4)	(5)	(6)	(7)	(8)	(9)	(10)	(11)
Tr 16-100	-5.00 ^b	0.30 ^b	8.52	2.18	1850	370
Tr 16-11	-5.63	2.44	-2.21	0.35	-3.42	2.47	11.20	1.61	4000	1970
Tr 16-115	-7.99	1.08	-2.87	0.06	-5.11	1.08	10.03	1.94	4370	950
Tr 16-12	-6.03	1.14	-2.84	0.14	-3.19	1.15	11.50	2.26	3060	710
Tr 16-122	-4.53	1.12	-2.23	0.23	-2.31	1.15	11.34	1.75	2400	550
Tr 16-124	-6.33	1.81	-2.84	0.13	-3.49	1.81	11.09	2.24	2940	1060
Tr 16-127	-7.47	1.16	-2.86	0.06	-4.61	1.16	10.67	2.77	3170	740
Tr 16-16	-5.15	4.77	-2.70	0.33	-2.45	4.78	10.75	2.09	1670	1590
Tr 16-17	-6.69	2.10	-2.72	0.38	-3.98	2.13	10.86	1.83	4000	1710
Tr 16-18	-5.62	1.08	-2.84	0.14	-2.78	1.09	12.11	1.65	4440	970
Tr 16-22	-4.30 ^b	0.30 ^b	10.85	3.51	2130	430
Tr 16-23	-4.65 ^b	0.30 ^b	10.00	2.91	2230	450
Tr 16-24	-4.29	1.12	-2.14	0.19	-2.16	1.14	11.51	1.72	2450	560
Tr 16-246	-6.49	1.99	-2.71	0.45	-3.78	2.04	11.92	2.98	3510	1430
Tr 16-26	-7.11	2.57	-2.39	0.45	-4.72	2.61	11.79	2.17	7390	3870
Tr 16-28	-5.21	1.03	-2.81	0.09	-2.39	1.03	11.57	1.93	2550	530
Tr 16-3	-7.19	0.98	-2.86	0.08	-4.33	0.98	10.12	1.89	3250	640
Tr 16-31	-6.79	0.97	-2.85	0.10	-3.94	0.97	10.47	1.89	3190	620
Tr 16-4	-6.05	1.23	-2.86	0.09	-3.18	1.24	11.17	1.79	3260	810
Tr 16-55	-4.87	1.25	-2.41	0.25	-2.47	1.28	12.19	1.97	3450	880
Tr 16-74	-5.70	1.11	-2.82	0.19	-2.87	1.13	11.61	2.14	2940	670
Tr 16-94	-4.53	0.93	-2.23	0.14	-2.31	0.94	9.91	1.30	1530	290

^a WEBDA^b Estimated based on spectral type following Walborn (1972).

REFERENCES

Alexander, M. J., Hanes, R. J., Povich, M. S., &
 McSwain, M. V. 2016, *AJ*, 152, 190

Berlanas, S. R., Herrero, A., Martins, F., et al.
 2017, *Highlights on Spanish Astrophysics IX*,
 453

- Damiani, F., Bonito, R., Magrini, L., et al. 2016, *A&A*, 591, A74
- Damiani, F., Klutsch, A., Jeffries, R. D., et al. 2017, arXiv:1702.04776
- Ekström, S., Georgy, C., Eggenberger, P., et al. 2012, *A&A*, 537, A146
- Elmegreen, B. G., & Lada, C. J. 1977, *ApJ*, 214, 725
- Flower, P. J. 1996, *ApJ*, 469, 355
- Gagné, M., Fehon, G., Savoy, M. R., et al. 2011, *ApJS*, 194, 5
- Getman, K. V., Feigelson, E. D., Kuhn, M. A., et al. 2014, *ApJ*, 787, 108
- Huang, W., & Gies, D. R. 2006, *ApJ*, 648, 580
- Kiminki, D. C., & Kobulnicky, H. A. 2012, *ApJ*, 751, 4
- Lanz, T., & Hubeny, I. 2007, *ApJS*, 169, 83
- Levato, H., Malaroda, S., Garcia, B., et al. 1991, *Ap&SS*, 183, 147
- Lyubimkov, L. S., Rostopchin, S. I., & Lambert, D. L. 2004, *MNRAS*, 351, 745
- Massey, P., DeGioia-Eastwood, K., & Waterhouse, E. 2001, *AJ*, 121, 1050
- Mohr-Smith, M., Drew, J. E., Napiwotzki, R., et al. 2017, *MNRAS*, 465, 1807
- Povich, M. S., Smith, N., Majewski, S. R., et al. 2011, *ApJS*, 194, 14
- Preibisch, T., Zeidler, P., Ratzka, T., Roccatagliata, V., & Petr-Gotzens, M. G. 2014, *A&A*, 572, A116
- Przybilla, N., Nieva, M.-F., & Butler, K. 2011, *Journal of Physics Conference Series*, 328, 012015
- Rebolledo, D., Burton, M., Green, A., et al. 2016, *MNRAS*, 456, 2406
- Sexton, R. O., Povich, M. S., Smith, N., et al. 2015, *MNRAS*, 446, 1047
- Smith, N., Povich, M. S., Whitney, B. A., et al. 2010, *MNRAS*, 406, 952
- Torres, G. 2010, *AJ*, 140, 1158
- Townsley, L. K., Broos, P. S., Corcoran, M. F., et al. 2011, *ApJS*, 194, 1
- Walborn, N. R. 1972, *AJ*, 77, 312